Monitoring Tropical Debris Covered Glacier Dynamics from High Resolution Unmanned Aerial Vehicle Photogrammetry, Cordillera Blanca, Peru

Oliver Wigmore[1,2,3,4], Bryan Mark[1,2]

5   [1]Department of Geography, The Ohio State University, Columbus OH, USA
[2]Byrd Polar and Climate Research Center, The Ohio State University, Columbus OH, USA
[3]Institute of Arctic and Alpine Research, University of Colorado Boulder
[4]Earth Lab, University of Colorado Boulder

Correspondence to: Oliver Wigmore (oliver.wigmore@colorado.edu)

10   **Abstract.** The glaciers of the Cordillera Blanca Peru are rapidly retreating and thinning as a result of climate change, altering the timing, quantity and quality of water available to downstream users. Furthermore, increases in the number and size of proglacial lakes associated with these melting glaciers is increasing potential exposure to glacier lake outburst floods (GLOFs). Understanding how these glaciers are changing and their connection to proglacial lake systems is thus of critical importance. Most satellite data are too coarse for studying small mountain glaciers and are often affected by cloud cover, while traditional airborne

15   photogrammetry and LiDAR are costly. Recent developments have made Unmanned Aerial Vehicles (UAVs) a viable and potentially transformative method for studying glacier change at high spatial resolution, on demand and at relatively low cost.

Using a custom designed hexacopter built for high altitude (4000-6000masl) operation we completed repeat aerial surveys (2014 and 2015) of the debris covered Llaca glacier tongue and proglacial lake system. High resolution orthomosaics (5cm) and digital

20   elevation models (DEMs) (10cm) were produced and their accuracy assessed. Analysis of these datasets reveals highly heterogeneous patterns of glacier change. The most rapid areas of ice loss were associated with exposed ice cliffs and melt water ponds on the glacier surface. Considerable subsidence and low surface velocities were also measured on the sediments within the pro-glacial lake, indicating the presence of extensive regions of buried ice and continued connection to the glacier tongue. Only limited horizontal retreat of the glacier tongue was observed, indicating that simple measurements of changes in aerial extent are

25   inadequate for understanding actual changes in glacier ice quantity.

1 Introduction

The Peruvian Andes hold around 70% of the world's tropical ice. Within Peru the Cordillera Blanca is the most glacierised mountain range with around 40% of Peru's glacier area (ANA, 2014). These glaciers are rapidly retreating primarily as a result of warming temperatures (Vuille et al., 2008; Vuille et al., 2003). Most recently Burns and Nolin (2014) calculated a 25% reduction

30   in glacier area from 1987 to 2010. Similarly, Racoviteanu et al., (2008) calculated a 22.4% reduction from 1970 to 2003 with an increase in the rate of retreat from 1970, they also determined that over this period the mean glacier terminus elevation increased by 113m. Glacier changes are altering downstream hydrology, changing water supply in terms of quantity, quality and timing (Baraer et al., 2009, 2012; Chevallier et al., 2011; Condom et al., 2011; Juen et al., 2007; Kaser et al., 2003; Rabatel et al., 2013). These changes have profound impacts on downstream communities, livelihoods and ecology (Bury et al., 2013, 2011; Carey et al.,

35   2014; Mark et al., 2010; Postigo et al., 2008; Young, 2009, 2014). Additionally, rapidly melting glaciers are increasing the number and volume of unstable proglacial lakes which represent a serious natural hazard through potential glacier lake outburst floods

(GLOFs) (Carey, 2008; Carey et al., 2012; Huggel et al., 2002; Lliboutry et al., 1977; Portocarrero, 2014). Understanding how these glaciers are changing, their connection to proglacial lake systems and the role of glacier surface heterogeneity in controlling melt processes is critical to inform future management and adaptation strategies. Unfortunately, current understanding has been limited due to the spatial and temporal resolution of available datasets and difficulties of accessibility to these remote mountain locations.

Processes of glacier melt and the formation of glacier lakes is controlled by a multitude of factors including local energy balance, topography, geology, aspect, valley dimensions, moraine stability, debris thickness and the presence of surface features such as melt ponds and ice cliffs (Benn et al., 2012; Buri et al., 2016; Harrison et al., 2006; Huggel et al., 2002; Immerzeel et al., 2014; Lejeune et al., 2013; Portocarrero, 2014; Reid et al., 2012; Reid and Brock, 2010; Thompson et al., 2012). The impact of these variables has been studied extensively in other areas, particularly the Himalaya, where large debris covered glacier tongues are common (Benn et al., 2012; Buri et al., 2016; Immerzeel et al., 2014; Scherler et al., 2011; Shroder et al., 2000). However, few detailed studies of these processes have focussed on the Cordillera Blanca. Remote sensing (satellite and airborne) has been widely used to quantify aerial changes in glacier extent for the Cordillera Blanca, and is routinely applied in national level inventories (ANA, 2014; Burns and Nolin, 2014). However, detailed studies of glacier melt processes and volumetric changes have not seen widespread use in the Cordillera Blanca due in part to the extreme topographic variation, generally small glacier size (typically less than 0.5km^2), and paucity of suitable datasets. Mark and Seltzer (2005) integrated DEM differencing and climate variables to investigate the role of aspect and elevation on glacier ablation. Huh et al., (2017) combined airborne LiDAR and photogrammetry to quantify changes in glacier volume for a handful of valleys within the Cordillera Blanca, but large errors exist for the earlier date photogrammetric DEM's. Most recently Emmer et al., (2015) combined a single DEM with high resolution satellite imagery and field investigations to understand the geomorphic evolution and measure surface velocities of the debris covered Jatunraju glacier. Most research in the Cordillera Blanca has addressed the entire range with a focus on glacier response to larger scale climatic perturbations (Rabatel et al., 2013; Vuille et al., 2008), and their role in the hydrologic budget of the Rio Santa basin (Baraer et al., 2012; Juen et al., 2007; Kaser et al., 2010). A number of studies have investigated mass balance response of individual glaciers, though these have generally aggregated mass balance at the glacier scale (Hastenrath and Ames, 1995a, 1995b; Kaser et al., 1990; Winkler et al., 2009). Few studies have documented glacier surface and volume changes at fine resolution in the Cordillera Blanca.

There are three primary methods for quantifying glacier change, glaciologic, hydrologic and geodetic (Cuffey and Paterson, 2010; Ostrem and Brugman, 1993). Only geodetic methods can provide detailed spatially continuous measurements of glacier surface changes. Geodetic methods rely on repeat remote sensing observations (satellite, airborne and terrestrial) to map surface characteristics, measure displacement velocities and vertical changes through differencing of digital elevation models (DEMs). Traditional methods of aerial remote sensing (satellite, airplane/helicopter) are constrained by three competing primary factors: spatial resolution, temporal resolution and cost. To make a gain in one of these factors there is a simultaneous loss in one or both of the other factors. Additionally, in mountain regions cloud cover is a notable issue as is safety for airborne platforms. However, recent developments in military, remote control, hobby and open source hardware have made it viable and potentially transformative to consider new small (1-5 kg), relatively inexpensive unmanned aerial vehicle (UAV) platforms for mapping glacier dynamics. UAV platforms include, helicopters, multi-rotors, fixed wings and paragliders; they are typically small (1kg - 5kg) and relatively cheap, ranging in cost from $400 to $40,000 (Eisenbeiß et al., 2009; Eisenbeiss and Sauerbier, 2011; Friedli, 2013). These platforms may be operated by remote control, first person or GPS enabled autopilot systems and can be fitted with a

diversity of sensors for collecting observations of the earth surface and atmosphere, including multispectral cameras, meteorology sensors and LiDAR units (Colomina and Molina, 2014; Hardin and Jensen, 2011; Nex and Remondino, 2014). Due to the low flight elevations (50 - 1000m above ground level) very high resolution imagery (<5cm pixels) can be collected from below the cloud level with limited risk to ground personnel or property. In addition these on-demand platforms can collect data at whatever temporal resolution is desired with no major additional acquisition costs.

In addition to these developments in UAV hardware, software developments have also occurred. Easy to use off the shelf software is now capable of processing large UAV image collections to derive orthomosaics and dense photogrammetric point clouds for the generation of DEMs. By integrating these data with differential GPS surveyed ground control points (GCP's) it is possible to generate DEMs with a ground resolution of under 5cm and orthomosaics of around 2cm resolution (Harwin and Lucieer, 2012; Hugenholtz et al., 2013). Accuracy of these datasets has been demonstrated to be very high in comparison to survey data and often equal or better than LiDAR (Harwin and Lucieer, 2012; Hugenholtz et al., 2013).

The use of UAVs in earth science research is undergoing rapid expansion with numerous researchers exploiting the financial and spatiotemporal resolution benefits of UAV technology (Ahmad, 2011; Colomina and Molina, 2014; D'Oleire-Oltmanns et al., 2012; Hardin and Jensen, 2011; Koh and Wich, 2012; Vivoni et al., 2014; Watts et al., 2012). A few projects have utilised UAV platforms in mountainous glaciated regions (Bhardwaj et al., 2016). Friedli (2013) has investigated their potential for glacier monitoring on the Rhone glacier, while Whitehead et al., 2013 conducted a detailed glacier study in the Canadian Arctic, however this was at low elevation. At higher elevations Immerzeel et al., (2014) and Kraaijenbrink et al., (2016) successfully used a small fixed wing platform to map glacier changes and surface velocities at 5000m in the Himalaya. Recently researchers have begun to explore the use of UAV's within the Cordillera Blanca, however, to our knowledge no published studies to date have deployed UAVs to study glacier dynamics within the Cordillera Blanca or the Tropical Andes.

2 Objectives

There are three principle objectives of this study:

1) Successfully deploy a multirotor platform suitable for mapping glacier changes and capable of operating at ~5000masl in mountainous terrain.
2) Measure glacier volume changes, surface velocities and proglacial lake changes at high resolution using decimetre DEM's and centimetre orthomosaics, and provide a quantitative assessment of their accuracy.
3) Use these data sets to investigate processes and patterns of glacier change over a debris covered glacier tongue and proglacial lake system in the Cordillera Blanca.

3 Study Area

The Cordillera Blanca is located in the central Andes of Peru (Fig. 1). The range extends 180km (north south) encompassing numerous peaks over 6000m, including Peru's highest, Huascaran at 6768m. The region contains more than 700 individual glaciers which terminate at over 4500masl. The climate is dominated by a strong wet/dry seasonal signal. The wet season corresponds to the austral summer (October-May) with roughly 80% of the 800-1200mm/yr of precipitation (Bury et al., 2011; Mark et al., 2010) falling over this time. As with other tropical mountain regions diurnal temperature variation greatly exceeds seasonal temperature variability (Kaser, 2001). Maximum ablation occurs at the same time as maximum accumulation during the wet season months

(Kaser, 2001). The focus of this study is Llaca glacier, which is located in the central Cordillera Blanca above the city of Huaraz (Fig. 1).

The Llaca valley is relatively narrow constricting to around 500m at its narrowest. The head of the valley opens into a large cirque over 3km wide with headwalls over 5500m and includes the summits of Ranrapalca (6162m) and Vallunaraju (5686m). Due to this large accumulation zone and narrow valley Llaca glacier extends to a considerably lower elevation (4500masl) than many other glaciers in the region which typically terminate between 4700-5100masl, for example Vallunaraju which shares a divide with Llaca and terminates at ~4800m (300m higher). The glacier snout is covered in a thick (>1m) layer of debris derived from the collapse of steep lateral moraines onto the glacier surface, which insulates the ice and also enables its extension to this lower terminal elevation. The lower debris covered tongue remains connected to the upper glacier and terminates in a moraine dammed and partially ice cored proglacial lake approximately 1km long, 0.2km wide and up to 17m deep (in 2004) storing an estimated 274300m^3 of liquid water (Portocarrero, 2014). The moraine dam underwent stabilisation and lowering (completed in 1977) as a component of the broader campaign within the Cordillera Blanca to mitigate the risk of glacier lake outburst floods (GLOF's) which have been responsible for a number of major natural disasters and large loss of life in the region (Carey, 2008; Carey et al., 2012; Lliboutry et al., 1977; Portocarrero, 2014). Lake stabilisation included construction of a reinforced concrete and steel dam within the terminal moraine and artificial lowering of the lake level. Despite these efforts a significant GLOF risk is still present due to avalanche risk from hanging glaciers above, tectonic activity and the location of this lake which drains to the Rio Santa through the northern edges of the city of Huaraz (Emmer and Vilímek, 2014; Portocarrero, 2014).

4 Methods

4.1 UAV platform design and specifications

A hexa-multirotor UAV was custom designed and built for this project (Fig. 2). The UAV is capable of operating at elevations between 3500 and 6000m above sea level. The 1m (diameter) frame utilises a lightweight carbon fibre construction and is fitted with high speed motors and 13 to 15 inch carbon fibre propellers (depending on flight altitude). All up weight excluding cameras is ~2kgs. Low weight is essential for operation at this altitude and eases transport when hiking/climbing to the glaciers. The maximum flight time for the platform at 5000masl is around 12-15 minutes on a single 10,000MAH 4S Lithium Polymer (LiPo) battery giving a range of 1.5-2.5km (depending on above ground flight altitude) from launch at flight speeds acceptable for aerial mapping (~8m/s). Autonomous navigation is managed by a 3DR Pixhawk flight controller. In comparison to fixed wing platforms; a multirotor platform sacrifices flight time in exchange for greater navigational precision, vertical takeoff and landing (essential over debris covered glacier surfaces and around water bodies), and typically higher quality images due to greater platform stability. Communication with the UAV is maintained with an extended range (2.5km) 2.4GHz radio controller (FrSky Taranis LR) and a long range (>40km) ~915MHz (RFD900+) telemetry link between the autopilot and ground station. Ground station control was managed by a field tablet running APM Mission Planner for Android (2014) and APM Mission Planner for Windows (2015).

The UAV was fitted with a single Canon S110 Powershot camera. The camera was installed in nadir view with no gimbal stabilisation. This camera allows full manual control of exposure settings including; ISO, F-stop, and shutter speed. The best settings are an ISO ~100-200 (to reduce image graininess), F-stop >4 (to improve depth of field), and shutter speed <1/1000s (to reduce motion blur). Camera control was managed by the Canon Hack Development Kit (CHDK). CHDK reboots the camera using firmware stored on the SD card and allows the use of custom scripts. In this case the kap_uav.lua script (CHDK, 2016) was

used. This script allows the specification of the camera parameters above and automatic image capture at set intervals. An interval of three seconds was selected to provide >90% image overlap, with additional redundancy for blurred image removal.

4.2 Ground control

Before each survey a comprehensive global navigation satellite system (GNSS) survey was conducted. This included installation
5 and survey of highly visible targets for use as ground control points (GCP's) in georectification of the photogrammetric point cloud and collection of 'check points' for accuracy assessment of derived DSM's (Fig. 2, Fig. 3, Table 1). Target installation points were distributed fairly evenly across the survey area making sure to include high and low points within the survey region. Access to the upper portion of the study area is very difficult and targets were unable to be installed here. Targets were anchored to the ground using metal stakes and rocks as appropriate to ensure they would not move before flights. Selection of check points was semi-
10 random making sure to include high and low points within the land surface. In 2014 points were taken atop and between individual rocks as well as over more uniform terrain. In 2015 check points were placed primarily in areas that exhibit relative terrain homogeneity within a roughly 50cm radius.

In 2014 base station data (for rover position correction) was collected with a Trimble 5700 receiver with a Zephyr Geodetic antenna
15 provided by UNAVCO, this was installed on an apartment roof in Huaraz (baseline ~14km) and occupied for almost 7 days collecting at 1Hz (Table 2). In 2015 base station data was collected with a Topcon Hiper-SR integrated receiver/antenna installed at the southern end of the moraine in Llaca valley (baseline ~1km) and occupied for 6.5 hours collecting at 1Hz. Base station positions were resolved using the Natural Resources Canada (NRCAN) Precise Point Positioning online service. Rover positions (targets and check points) were observed for 5 minutes at 1Hz frequency following a stop-go post processing workflow,
20 observations were collected using a Topcon GRS1 L1 receiver with a PG-A1 external antenna (Table 2). Following data collection all points were processed using Topcon Magnet^{TM} Office Tools (version 2.7.1) software with base station coordinates adjusted as per NRCAN positioning results.

4.3 Aerial survey flight paths

Flight planning was completed in the office using mission planner software and Google Earth. As the UAV is does not have
25 collision avoidance it is critical to carefully plan a flight path that avoids topographic obstacles such as moraine walls, cliffs etc, especially considering that for much of the survey the UAV would be flying beyond line of sight. Much of Google Earths topographic data relies on SRTM90, this dataset is too coarse resolution and often out of date (collected in 2000) for near surface navigation in the dynamic and heterogeneous terrain of the Cordillera Blanca. Additionally, limited sky view and possible dropped satellites present real navigational threats for the UAV itself. Therefore, an above ground level (agl) of ~100m was selected; as
30 this would provide sufficient ground resolution (~3cms) while also keeping the UAV well above the moraine walls (Fig. 3, Table 3). To maintain this above ground altitude the flight plan required the UAV to first ascend to 100m, then gain an additional ~200m as it moved up the valley over the glacier. This also maintains a uniform ground resolution. Five flight lines were constructed from the launch point below the calving face, to provide ~60% sidelap which is necessary for robust DEM recovery (Fig. 3). The maximum length of an individual flight line was 1.2km from the take off point, resulting in a total (return) flight length of roughly
35 2.5km. Total flight time was around 12mins per flight travelling at ~8m/s. Rapid battery drain was experienced in the take-off portion and when gaining altitude up valley which limited the range and thus the total survey-able region.

4.4 Structure from motion workflow - DEM and orthomosaic generation

Collected image data were processed using the Structure from Motion (SfM) workflow as implemented in Agisoft PhotoScan Professional Edition (Version 1.1) (Agisoft, 2016). This is proprietary software thus the specific algorithms used are not available. However, the basic principles outlined below are similar across all commercial and open source software packages. Further details on SfM can be found in Fonstad et al., (2013), Lowe, (2004), Snavely et al., (2008), Szeliski (2010) and Verhoeven, (2011).

1. A feature recognition algorithm is used to identify unique tie points across the image data set, e.g. scale invariant feature transform (SIFT) (Lowe, 2004).
2. A bundle block adjustment is performed to reconstruct camera positions and construct a sparse point cloud.
3. Ground control targets are identified within the scene and positioned on each individual photo in which they are visible. Placement accuracy of individual markers is within ~3cm (width of the X on targets).
4. The following step is iterated three times to reduce model error as estimated by the software. Sparse point cloud is optimised to fit ground targets. Points with estimated reprojection error >1.5cm are deleted. Repeat.
5. A dense point cloud is generated from the sparse point cloud model.
6. A 3D model, raster DSM and orthomosaics are output for analysis.

For this study DEMs were generated at 10cm pixel resolution and RGB orthomosaics were created at 5cm pixel resolution.

4.5 Accuracy assessment

Accuracy of the DEM's is estimated in two ways. Firstly, the photogrammetric software provides a number of different error statistics including tie point matching error and GCP placement error (difference between actual coordinates and estimated position from SfM processing) (Table 4). These parameters describe how well the point cloud and camera positions fit the in scene ground targets. Error is provided as RMSE, xyz differences and pixel matching errors. These errors are reduced within the SfM workflow by optimising the point cloud while minimising potential position variance from control points. Outliers are selected and removed through a few iterations to reduce error estimates. Secondly, the surveyed GPS elevation at the check point locations is compared against the elevation extracted from the DEM surface providing a more precise estimate of absolute elevation error for each surface. A third method for estimation of error is to compare difference in the DSM elevations over regions that have experienced no change. Unfortunately no regions within the study area were identified that could be assured not to have undergone elevation change over the study period. This method was therefore not used.

4.6 Elevation change, surface velocity and orthomosaic comparison

Analysis of glacier changes was conducted in ESRI Arc Map 10.2. Volumetric change was calculated for the entire survey area and the debris covered glacier section separately. This was done by clipping the DEM's to the glacier boundary and subtracting the 2014 DEM from the 2015 DEM; i.e. negative values equal elevation drop/ice loss. Surface velocity was determined by manual feature tracking of 72 points on the glacier tongue to produce velocity vectors. Following vector creation a velocity surface was interpolated for the glacier tongue using the spline interpolation tool in Arc Map. To investigate melt patterns across the glacier surface horizontal movement must be removed so that the same area of the glacier surface is compared. To do this the velocity vectors above were used to orthorectify the 2015 orthomosaic to the same location as the 2014 orthomosaic. Vectors of ice cliff movement were then calculated between the two dates. Within the lake section of the survey area elevation changes of water bodies were measured and ice cored regions were investigated, as well as limited feature tracking to estimate horizontal movement.

5 Results

5.1 GNSS and DEM accuracies

Base station positions were located with an estimated combined (horizontal and vertical) error of 0.5cm (2014) and 7cm (2015) (Table 2). Positional errors of the GCP's and check points are all estimated to be under 2.5cm (2014) and 0.6cm (2015) (Table 2).

5 Providing an estimated combined positional error of 3cm (2014) and 8cm (2015). Thus maximum expected errors in positions compared between the two dates are ~11cm. 2014 rover positions are less accurate due to the long (15km) baseline, however the longer base station occupation interval means they are overall better constrained. Rover positions in 2015 are more accurate due to a shorter (1km) baseline but the base station position is less accurate due to a much shorter occupation interval (6.5hrs versus almost 7 days) (Table 2). This could not be avoided as the base station could not be left in place overnight due to security concerns.

Estimated tie point (image) matching errors are summarised in Table 4, with a mean value of 0.63 pixels (at 3.5cm pixel size (Table 3)) for 2014 and 0.43 pixels (at 3.6cm pixel size (Table 3)) for 2015. Errors in both cases are sub pixel at the minimum pixel size; these results are improved when the DEM and orthomosaics are aggregated for analysis to 10cm and 5cm respectively. Additional error estimates are provided as the measured difference (in metres and pixels) between GCP coordinates and estimated GCP

15 position within the SfM model (Table 4). These errors are sub centimetre for both years; 0.002m in 2014 and 0.003m in 2015. The error statistics provided above however tend to overestimate DEM accuracy. DEM accuracy should therefore be assessed by either comparing differences over no change areas or comparing to additional survey points not used in generating the DEM.

To gain a better understanding of the absolute accuracy of the two DEM surfaces elevations from the DEM were compared against

20 those from check points surveyed in their respective years (Fig. 3, Fig. 4). The results of this analysis are summarised in Fig. 5 and Fig. 6. Mean difference between DEM and GNSS check points in 2014 is -0.037m with a standard deviation of 0.191m; in 2015 mean difference is 0.001m with a standard deviation of 0.044m. Negative values indicate underestimation of DEM surface with respect to surveyed positions and thus imply flattening of the DEM surface. Most errors are less than +/-5cm, and are the combined result of errors in image matching/SfM processing, GNSS positional errors and DEM smoothing of small surface features. The

25 2014 data have a much larger error range than in 2015, however this is deemed to be the result of experimental error as opposed to true inaccuracies in the DEM surface. In 2014 check points were collected in areas of non uniform topography, i.e. atop rocks, between cracks etc, these minor topographic features are smoothed out of the DEM resulting in a larger difference between GNSS and DEM elevations. In 2015 check points were located in areas with only minor topographical variation within a roughly 0.5m radius therefore the impacts described above are minimised and estimated accuracy is higher.

30 **5.2 Measured changes over the survey area**

Changes in surface elevation were highly variable across the survey area, including areas of both loss and gain (Fig. 7). Over the glacier tongue (blue boundary Fig. 7) the mean elevation change was -0.75m from 23 July 2014 to 28 July 2015. This equates to 156,000 m^3 of ice loss. The standard deviation is 2.58m, with a minimum value of -18m and a maximum value of +11.5m, however, from Figure 8 it is evident that almost all values are within -10m to +7.5m. Notably, despite this reduction in ice volume the glacier

35 terminus position (and thus area) remained essentially unchanged between the survey dates. Surface velocities range from 27m/yr to 4m/yr from the upper glacier to the calving face respectively. There is a roughly linear decrease in velocity down glacier, due to the relatively uniform slope. However, minor variations are evident (Fig. 7c), these correspond to variations in gradient, with

steeper slopes resulting in increased flow velocity. Higher ice velocities also coincide with regions experiencing reduced rates of ice loss and/or some limited gains in elevation. Similarly, gentler slopes coincide with higher rates of ice loss.

The largest elevation change of 18m of ice loss was measured at the calving face (Fig. 9, Fig. 10). The greatest measured increase in surface elevation is the result of a large boulder moving down glacier between the survey dates (Fig. 9), other areas of elevation increase are also primarily associated with the downward movement of large surface features. Apart from the calving face the most dramatic areas of surface ablation are associated with exposed ice cliffs and melt ponds (Fig. 9, Fig. 11). Figure 11 shows the horizontal movement and expansion of these ice cliffs and the retreat of the calving face (note: the 2015 image has been georectified to remove any horizontal glacier movement based on calculated velocity vectors, see Fig. 7). Rates of horizontal retreat measured for these features range from 2m to 25m/yr with larger cliffs retreating more rapidly. Appearance, expansion and disappearance of melt ponds is also visible in the imagery.

Figure 12 shows the mean, and standard deviation of elevation changes measured within 10m altitude bands over the glacier tongue. Mean elevation change for the lowest altitude band (4480-4490m) is the highest at -10.4m due to collapse of the calving face. Variability (standard deviation) in mean ice loss is also highest for this section. Mean ice loss is greatest for elevations below 4530m, or roughly the lowest half of the glacier tongue, and generally decreases moving up the glacier tongue. From Figure 12 we can also see there is some connection between highest mean mass loss and the slope of the glacier (contour spacing). Ice emergence as a result of higher ice velocities over slightly steeper sections may be responsible for the observed slight increases in mean elevation (ice gain) for these steeper slopes (Fig. 7 and Fig. 12).

Considerable changes were also measured within the proglacial lake system below the calving face. The lake system can be divided into two parts. The lower section comprises the main (larger) lake and is the section for which the glaciology office has completed bathymetric surveys and volume assessments (Portocarrero, 2014). This section was not surveyed and likely experiences limited change as its water level is controlled by the dam culvert. The upper section between the lake and the calving face includes numerous smaller ponds interspersed with debris piles. Within this upper lake section numerous changes were observed over the survey period. Noticeable changes in the arrangement and size of the surface ponds occurred, with new ponds forming and others disappearing between the survey dates (Fig. 13). The elevation of these ponds varies greatly, with some sitting up to 4m above the main lakes elevation of 4480masl. The largest pond is 15,000m^2 and lies ~2.5m above the main lake. Additionally, two locations experienced large elevation changes with surface lowering of 5-10m recorded over the study period (Fig. 13), suggesting the presence of buried blocks of remnant glacial ice within the sediments. Low velocities of approximately 2.5m/yr were also measured close to the calving face decreasing to ~0.5m/yr at the southern edge of the surveyed area.

6 Discussion

6.1 Glacier and proglacial lake dynamics

Surface melt patterns over the glacier tongue were remarkably varied across small spatial scales, though generally ice loss was higher at lower elevations, presumably as a result of slightly higher temperatures (Fig. 12). The largest amount of ice loss occurred at the calving face where a major collapse took place between the two survey dates (Fig. 8 and Fig. 9). From speaking with local climbing guides much of this loss occurred over a roughly two week period in March-April 2015. In the region behind the calving face considerable down wasting (roughly 1m to 8m) occurred likely as a direct result of the calving face collapse, which had

previously provided a buttressing effect for the ice behind. No notable changes in glacier area or terminus positon were measured between the two survey dates, despite the large reduction in ice volume (156,000 m^3 of ice loss). This finding illustrates the importance of measuring volume changes and not just areal changes within the Cordillera Blanca. Elsewhere the highest melt rates were associated with ice cliffs and surface ponds (Fig.11). Exposed ice cliffs lack the insulation of thick debris cover and thus are

5   exposed directly to intense incoming solar radiation at high altitude in the low latitudes, and thus experience rapid melting and horizontal recession across the glacier surface (Fig. 11) (Buri et al., 2016; Sakai et al., 1998, 2000). At the Lirung glaciers debris covered tongue in Nepal, Sakai et al., (1998) observed an ice cliff horizontal retreat rate of 15-44m/yr (4-12cm/day), more recently Buri et al., (2016) measured a rate of 11-18m/yr (3-5cm/day) for the same glacier. This is comparable to the 2-25m/yr observed at Llaca glacier. Surface melt ponds have a lower albedo than exposed ice and therefore warm up rapidly; enhancing melt processes

10   and increasing melt pond size (Sakai et al., 2000). It is probable that the two features are closely related through the following process. Surface melt ponds develop at low points on the glacier surface where surface melt water collects, this raises surface albedo enhancing melt and expanding the pond. As the pond expands and deepens ice cliffs develop around it, then as they steepen lose their debris cover and begin to recede rapidly across the glacier surface. A number of surface melt ponds disappeared between the two survey dates, which indicates potential subglacial drainage pathways through englacial conduits (Benn et al., 2012).

15   Immerzeel et al., (2014) identified similar features through analysis of UAV datasets collected over a debris covered glacier in the Himalaya, and associated their presence with ice cliffs. The fine scale of these surface features could not be resolved using medium and coarse resolution satellite imagery and would be extremely labour intensive to observe with in situ measurements.

Apart from areas of ice cliffs and melt ponds the glacier is covered in a thick debris layer. Going back to Ostrem, (1959) numerous

20   studies have investigated the role of debris cover in either enhancing ablation through reduced albedo when debris cover is thin, or reducing ablation when debris cover is sufficiently thick to have an insulative effect (Juen et al., 2014; Pratap et al., 2015; Shahi et al., 2015). No detailed measurements of debris thickness and distribution were collected for this study, however, field observations suggest it was generally in excess of 1m thick and composed of mixed sediment sizes from silts and fine sands through boulders over 1m in diameter. Thus, Llaca's debris cover is probably sufficiently thick that it primarily provides an insulative

25   effect for the ice beneath. The insulative effect of the debris cover is at least in part responsible for its low terminus elevation of 4500m, some 200-600m lower than many of the other glaciers in the region. Additional, factors probably include, the large accumulation zone within a high elevation cirque over 6000m high; a narrow valley width which restricts width of the glacier tongue, increasing length and thickness; and, perhaps a greater degree of surface shading than in some of the wider valleys. Thus it appears that debris thickness or the lack there of is the primary control on measured ablation rates for the tongue of Llaca glacier.

30   Where debris cover is absent (ice cliffs) or melt ponds are present ablation rates are dramatically increased, while in areas of thick debris cover insulation of the ice surface dominates, reducing melt rates. The interplay of these processes across the glacier surface is responsible for the high degree of spatial heterogeneity observed in glacier melt patterns and the complex topography of the tongues surface.

35   Many sections of the glacier tongue show a gain in surface elevation (Fig. 7). These however are not zones of accumulation and can instead be explained primarily by the highly irregular nature of the glacier surface. The glacier surface has numerous surface irregularities including topographic undulations, cliffs and large boulders. As the glacier moves downslope these surface features move through the scene thus elevation comparisons at an individual point are not actually comparing the same point on the glacier surface (which has moved) but instead compare the same position in real world coordinates. Therefore if a large boulder or surface

40   feature moves down slope it will be measured as an increase in surface elevation at its new position. The inverse effect (elevation

loss) can occur as large depressions move through the scene. Examples of this can be seen in Figure 10 where a large boulder roughly 10m high moves down slope producing a measured elevation decrease at is location in 2014 and a measured elevation increase at its location in 2015. Care must therefore be taken when comparing measurements of vertical change at a specific location. This is not an issue faced by non geodetic methods such as ablation stakes which move with the glacier and thus provide

5   a measure of actual ablation at that position on the glacier surface. Vertical emergence may also contribute to the observed increases in ice elevation. There do appear to be some minor increases in measured elevation and/or lower ablation in areas of steeper slope (Fig. 12) and faster velocities (Fig. 7) suggesting some limited emergence could be occurring in these regions, presumably driven by bed topography. However, any emergence is likely to be limited as the glacier bed in the study section is likely fairly smooth and of relatively uniform gradient, additionally the glacier in this section undergoes no notable direction changes that could produce

10   large emergence velocities. Therefore the impacts of emergence in creating these observed elevation increases is likely minimal.

Very few measurements of glacier surface velocities are reported for the Cordillera Blanca. Emmer et al., (2015) reported maximum values of 11.2m/yr for a similar debris covered section at the much steeper Jatunraju glacier, which is less than half what is presented here. However, the relative size of the accumulation area at Llaca is much larger than for Jatunraju. It is also possible

15   that the glacier/bedrock interface is somewhat lubricated through contact with the proglacial lake, potentially increasing horizontal velocity. The observed decrease in velocity down glacier is essentially linear. As the surface gradient is fairly constant over the glacier tongue (Fig. 7) this velocity reduction is likely due to a reduction in ice mass closer to the glacier terminus which is in part a result of the higher melt rates occurring over the lower sections of the glacier tongue.

20   The upper section of the proglacial lake was surprisingly dynamic, with a number of major changes occurring between the two survey periods, including the expansion and disappearance of ponds, and large areas of subsidence (5-10m/yr).These changes suggest that sediments within the lake system are interspersed with buried chunks of remnant glacier ice which is slowly melting. As these ice remnants melt, surface and subsurface hydrologic connections can open and close impacting the size and distribution of surface ponds and changing the surface topography. The variation in pond elevation and up to 4m offset above the main lake,

25   indicates that they are separate hydrologic features from one another, and from the main lake, as opposed to a single connected lake system. Drainage of these ponds is likely rapid, as surface and subsurface channels open due to the melt of buried ice bodies, and through the impacts of waves triggered by talus falls from the lateral moraine and calving of the glacier tongue. Low surface velocities were also measured within this section ranging from 2.5m/yr below the calving face to 0.5m/yr at the end of the survey area where the main lake starts. These low velocities suggest that the sediments below the calving face are still being actively

30   pushed down valley by the glacier. It is also possible that some direct ice connection to the main glacier remains, buried below the surface sediments.

Measured changes within the proglacial lake sediments illustrate that this system is actively evolving as a result of continued ice melt. As this process continues the extent and depth of the main lake will increase. While no change in the glacier terminus was

35   measured in this study, 18m of down wasting occurred at the calving face, as this down wasting continues the proglacial lake will eventually expand north-eastward. The Huaraz glaciology office estimated the main lake to hold ~274300m^3 of water in 2004 (Portocarrero, 2014). From an inspection of the surrounding topography and comparison with other proglacial lakes in the Cordillera Blanca it appears the lake could expand some 600m to 1000m further northeast as the glacier gradually disappears, potentially doubling in area. This larger lake will be in closer proximity to the steep headwalls of the valley, which are potential

40   locations for avalanche and rock fall debris that are triggers for GLOF hazards. Emmer and Vilímek's, (2014) assessment of the

GLOF risk at Llaca defines this as the most likely risk scenario for this lake. Presently the risk of a large GLOF is limited, as any major rock fall and/or avalanche debris would land atop the glacier tongue. However, rapid drainage of perched melt water ponds (the largest of which is 15,000m² and sits ~2.5m above main lake) within this upper lake section could produce rapid fluctuations in water inputs to the main lake. Large rapid inflows to the main lake have the potential to impact downstream infrastructure such as the moraine dam, power generator and water diversions in the valley below.

6.2 Benefits and challenges of UAVs for glacier mapping

UAVs are capable of providing centimetre resolution imagery on demand, at low cost, with the potential to provide unique insights into spatiotemporal dynamics of the cryosphere. The ease and relatively low cost of collecting highly accurate repeat DEMs makes UAVs a particularly suitable system for the geodetic assessment of glacier changes and mass balance calculation. UAVs are especially suited to the study of mountain glaciers where steep topography, frequent cloud cover, surface heterogeneity, and generally smaller glacier size (as compared to ice sheets) can limit the use of satellite imagery. Furthermore, UAVs are able to access and accurately survey potentially dangerous areas of the glacier surface (e.g. avalanche paths). In this study we exploited the spatial resolution of UAV datasets to analyse annual changes, however it is necessary to point out the suitability of UAVs for rapid return surveys over short temporal intervals. It is entirely feasible to complete weekly, daily or even diurnal surveys of the glacier surface, which could provide unique insights into glacier processes that are near impossible to obtain with other technologies. Similarly, multispectral, hyperspectral and thermal imaging sensors could be deployed to provide further insights into debris thickness distribution (Schauwecker et al., 2015), surface and melt pond albedo, and, surface energy processes (Aubry-Wake et al., 2015). The application of UAVs to glaciology is just beginning, however there are a few significant limitations to the methods described in this paper which are addressed below.

To generate high accuracy DEMs in scene ground control targets must be installed and surveyed. To minimise distortions in the SfM processing workflow these GCPs should be well distributed across the glacier surface, particularly at the survey margins where 'fishbowling' of the DEM can occur due to the propagation of SfM modelling errors. However, installing GCPs across a glacier is extremely labour intensive, and in many cases is highly dangerous or impossible without considerable mountaineering experience. A possible solution to this is through the integration of real time kinematic (RTK) GNSS positioning on the UAV platform. If the camera positions are accurately known in real world coordinates (including latitude, longitude elevation, pitch, roll and yaw) then GCPs are unnecessary for derivation of the DEM through SfM processing. These parameters can be added to image metadata by integrating the sensor package and autopilot/GNSS equipment. However, as the UAV is moving quickly (~8m/s) even a slight delay between camera trigger time and the RTK position can produce significant errors. These may not be an issue for single surveys of the land surface (e.g. crop mapping), however, when repeat DEMs are to be used for assessment of surface change horizontal and vertical accuracy of the DEMs is critical. Furthermore, the addition of RTK GNSS to the UAV increases cost and more importantly weight which reduces flight time. Despite these potential issues we believe the integration of RTK positioning on board the UAV platform is a necessary addition for the operational deployment of UAVs for glacier monitoring. Thankfully, RTK systems are rapidly reducing in price, with the entry of numerous low cost and UAV specific options coming to market in recent years, which will facilitate greater availability of these systems. Another way to reduce DEM error is through survey design. Firstly, overlap and side-lap can be increased, though the later increases flight line density and thus total survey time. Secondly, a crosshatch survey grid pattern can be employed which may improve SfM processing accuracy and reduce distortions at the survey periphery. Though deploying a crosshatch grid doubles survey time, which may be unfeasible.

An additional constraint is the maximum survey-able area. Maximum survey area is limited by the total flight time on a single battery. Lower air density at higher elevations significantly reduces propeller generated lift and negatively impacts maximum flight time. For example, the platform used in this study is capable of approximately 25 minutes of flight time at sea level but only 12 minutes of flight time at 5000m. With only 12 minutes of flight time the maximum range for this platform is around 1.5 to 2.5km

5   from the launch point flying at a suitable survey speed (around 8m/s) depending on local wind conditions and flight altitude above ground. Thus, the potential for deploying multirotors to map large glaciers at high elevations is limited. Fixed wing platforms are capable of considerably longer flight times (>1hr), however, multirotors are easier to fly, can land in a smaller location, can better navigate variable terrain features and are generally more stable in variable winds. Due to the complex terrain of mountain environments, often rough landing conditions and frequently strong gusty winds multirotors may be the preferred and safer option

10   for many studies. However, the trade-offs between maximum survey area and local conditions should be carefully considered before deciding on a suitable platform.

7 Conclusion

This study deploys a custom designed hexacopter UAV to map dynamics of a debris covered glacier tongue in the Cordillera Blanca, Peru. To our knowledge it is the first time a UAV has been deployed for this purpose in the tropical Andes and is the

15   highest altitude deployment of a multirotor UAV for mapping purposes in the current literature. We completed repeat aerial surveys (23 July 2014 and 28 July 2015) of the glacier tongue and proglacial lake system. Using a SfM workflow we generated highly accurate 10cm DEM's and 5cm orthomosaics. Analysis of these data reveals heterogeneous changes in the glacier surface with some areas of the glacier losing as much as 18m of vertical elevation due to collapse of the calving face. Average glacier down wasting was -0.75m over the study period or roughly 156,000m^3 of ice loss. The most rapid areas of ice loss were associated with

20   exposed ice cliffs and melt water ponds on the glacier surface. Surface velocities were recovered from manual feature tracking and ranged from 27m/yr in the upper surveyed section to around 4m/yr at the calving face. Surface lowering and low surface velocities were also measured over the sediments within the proglacial lake indicating that extensive regions of glacier ice remain buried within the lake sediments that are still connected horizontally to the glacier tongue. Only limited horizontal retreat of the glacier tongue was recorded thus simple measurements of changes in aerial extent can provide only a limited understanding of actual

25   changes in glacier ice. Continued down wasting of the glacier surface and melting of buried ice within the proglacial lake sediments will increase the size of the proglacial lake over time. As the lake boundary migrates towards the valley headwall GLOF risks associated with avalanches from the cirque above are likely to increase.

This study achieves two primary goals. Firstly, it clearly illustrates the viability and suitability of this technology for studying high

30   resolution changes in mountain glaciers, and the feasibility of operating multirotors at high elevation (>5000m). Secondly, it provides insights in to the processes that control glacier melt over a debris covered tropical glacier. Our findings regarding the importance of ice cliffs and surface melt ponds in debris covered glacier melt processes corroborate findings for debris covered glaciers in the Cordillera Blanca (Emmer et al., 2015) and the Himalaya (Buri et al., 2016; Immerzeel et al., 2014). The high spatial resolution of UAV derived datasets facilitates a much better understanding of surface heterogeneity and spatial variability in debris

35   covered glacier melt processes and changes in proglacial lake systems. UAV's offer a low cost on demand alternative to existing technologies, they can provide unique insights into dynamic earth system processes and are ideal for small scale studies in complex mountain regions.

Acknowledgements

This study was co-funded by NSF Grants: DEB-1010550 and BCS-1434248, The American Philosophical Society, The American Geographical Society, The Explorers Club, The Geological Society of America and The Ohio State University Office of International Affairs. Additional support in the form of GNSS equipment loan for 2014 was provided by the UNAVCO Facility with support from the National Science Foundation (NSF) and National Aeronautics and Space Administration (NASA) under NSF Cooperative Agreement No. EAR-0735156. Permission to operate the UAV within the Huascaran National Park was provided by the Parque Nacional Huascaran Office in Huaraz.

References

Agisoft: Agisoft PhotoScan User Manual Standard Edition, Version 1.2, St. Petersbg. Agisoft LLC [online] Available from: http://www.agisoft.com/pdf/photoscan_1_2_en.pdf, 2016.

Ahmad, A.: Digital mapping using low altitude UAV, Pertanika J. Sci. Technol., 19(June), 51–58, 2011.

ANA: Inventario Nacional de Glaciares y Lagunas., 2014.

Aubry-Wake, C., Baraer, M., McKenzie, J. M., Mark, B. G., Wigmore, O., Hellström, R. Å., Lautz, L. and Somers, L.: Measuring glacier surface temperatures with ground-based thermal infrared imaging, Geophys. Res. Lett., 42(20), doi:10.1002/2015GL065321, 2015.

Baraer, M., McKenzie, J. M., Mark, B. G., Bury, J. and Knox, S.: Characterizing contributions of glacier melt and groundwater during the dry season in a poorly gauged catchment of the Cordillera Blanca (Peru), Adv. Geosci., 22, 41–49, doi:10.5194/adgeo-22-41-2009, 2009.

Baraer, M., Mark, B. G., Mckenzie, J. M., Condom, T., Bury, J., Huh, K. I., Portocarrero, C., Gómez, J. and Rathay, S.: Glacier recession and water resources in Peru's Cordillera Blanca, J. Glaciol., 58(207), 134–150, doi:10.3189/2012JoG11J186, 2012.

Benn, D. I., Bolch, T., Hands, K., Gulley, J., Luckman, A., Nicholson, L. I., Quincey, D., Thompson, S., Toumi, R. and Wiseman, S.: Response of debris-covered glaciers in the Mount Everest region to recent warming, and implications for outburst flood hazards, Earth-Science Rev., 114(1–2), 156–174, doi:10.1016/j.earscirev.2012.03.008, 2012.

Bhardwaj, A., Sam, L., Martín-torres, F. J. and Kumar, R.: Remote Sensing of Environment UAVs as remote sensing platform in glaciology : Present applications and future prospects, Remote Sens. Environ., 175, 196–204, doi:10.1016/j.rse.2015.12.029, 2016.

Buri, P., Pellicciotti, F., Steiner, J. F., Miles, E. S. and Immerzeel, W. W.: A grid-based model of backwasting of supraglacial ice cliffs on debris-covered glaciers, Ann. Glaciol., 57(71), 199–211, doi:10.3189/2016AoG71A059, 2016.

Burns, P. and Nolin, A.: Using atmospherically-corrected Landsat imagery to measure glacier area change in the Cordillera Blanca, Peru from 1987 to 2010, Remote Sens. Environ., 140, 165–178, doi:10.1016/j.rse.2013.08.026, 2014.

Bury, J., Mark, B. G., Carey, M., Young, K. R., Mckenzie, J. M., Baraer, M., French, A. and Polk, M. H.: New geographies of water and climate change in Peru : Coupled natural and social transformations in the Santa River watershed, Ann. Assoc. Am. Geogr., 103(September 2015), 363–374, doi:10.1080/00045608.2013.754665, 2013.

Bury, J. T., Mark, B. G., McKenzie, J. M., French, A., Baraer, M., Huh, K. I., Zapata Luyo, M. A. and Gómez López, R. J.: Glacier recession and human vulnerability in the Yanamarey watershed of the Cordillera Blanca, Peru, Clim. Change, 105(1), 179–206, doi:10.1007/s10584-010-9870-1, 2011.

Carey, M.: Disasters, development, and glacial lake control in twentieth-century Peru, in Mountains: Sources of Water, Sources of Knowledge, pp. 181–196, Springer., 2008.

Carey, M., Huggel, C., Bury, J., Portocarrero, C. and Haeberli, W.: An integrated socio-environmental framework for glacier hazard management and climate change adaptation: Lessons from Lake 513, Cordillera Blanca, Peru, Clim. Change, 112(3–4), 733–767, doi:10.1007/s10584-011-0249-8, 2012.

Carey, M., Baraer, M., Mark, B. G., French, A., Bury, J., Young, K. R. and McKenzie, J. M.: Toward hydro-social modeling: Merging human variables and the social sciences with climate-glacier runoff models (Santa River, Peru), J. Hydrol., 518(PA), 60–70, doi:10.1016/j.jhydrol.2013.11.006, 2014.

CHDK: KAP UAV Exposure Control Script, [online] Available from: chdk.wikia.com/wiki/KAP_UAV_Exposure_Control_Script, 2016.

Chevallier, P., Pouyaud, B., Suarez, W. and Condom, T.: Climate change threats to environment in the tropical Andes: Glaciers

and water resources, Reg. Environ. Chang., 11(SUPPL. 1), 179–187, doi:10.1007/s10113-010-0177-6, 2011.

Colomina, I. and Molina, P.: Unmanned aerial systems for photogrammetry and remote sensing: A review, ISPRS J. Photogramm. Remote Sens., 92, 79–97, doi:10.1016/j.isprsjprs.2014.02.013, 2014.

Condom, T., Escobar, M., Purkey, D., Pouget, J. C., Suarez, W., Ramos, C., Apaestegui, J., Zapata, M., Gomez, J. and Vergara, W.: Modelling the hydrologic role of glaciers within a Water Evaluation and Planning System (WEAP): a case study in the Rio Santa watershed (Peru), Hydrol. Earth Syst. Sci. Discuss., 8(1), 869–916, doi:10.5194/hessd-8-869-2011, 2011.

Cuffey, K. M. and Paterson, W. S. .: The Physics of Glaciers 4th Edition, 4th ed., Academic Press., 2010.

D'Oleire-Oltmanns, S., Marzolff, I., Peter, K. D. and Ries, J. B.: Unmanned aerial vehicle (UAV) for monitoring soil erosion in Morocco, Remote Sens., 4(11), 3390–3416, doi:10.3390/rs4113390, 2012.

Eisenbeiss, H. and Sauerbier, M.: Investigation of UAV systems and flight modes for photogrammetric applications, Photogramm. Rec., 26(136), 400–421, doi:10.1111/j.1477-9730.2011.00657.x, 2011.

Eisenbeiß, H., Zurich, E. T. H., Eisenbeiß, H. and Zürich, E. T. H.: UAV photogrammetry, ETH Zurich, Switzerland:, 2009.

Emmer, A. and Vilímek, V.: New method for assessing the susceptibility of glacial lakes to outburst floods in the Cordillera Blanca, Peru, Hydrol. Earth Syst. Sci., 18(9), 3461–3479, doi:10.5194/hess-18-3461-2014, 2014.

Emmer, A., Loarte, E. C., Klimeš, J. and Vilímek, V.: Recent evolution and degradation of the bent Jatunraju glacier (Cordillera Blanca, Peru), Geomorphology, 228, 345–355, doi:10.1016/j.geomorph.2014.09.018, 2015.

Fonstad, M. A., Dietrich, J. T., Courville, B. C., Jensen, J. L. and Carbonneau, P. E.: Topographic structure from motion: a new development in photogrammetric measurement, Earth Surf. Process. Landforms, 38(4), 421–430, doi:10.1002/esp.3366, 2013.

Friedli, E.: Photogrammetric Methods for the Reconstruction and Monitoring of Glaciers, Master's Thesis, ETH Zürich, Zürich, Switzerland., 2013.

Hardin, P. J. and Jensen, R. R.: Small-scale unmanned aerial vehicles in environmental remote sensing: challenges and opportunities, GIScience Remote Sens., 48(1), 99–111, doi:10.2747/1548-1603.48.1.99, 2011.

Harrison, S., Glasser, N., Winchester, V., Haresign, E., Warren, C. and Jansson, K.: A glacial lake outburst flood associated with recent mountain glacier retreat, Patagonian Andes, The Holocene, 16(4), 611–620, doi:10.1191/0959683606hl957rr, 2006.

Harwin, S. and Lucieer, A.: Assessing the accuracy of georeferenced point clouds produced via multi-view stereopsis from unmanned aerial vehicle (UAV) imagery, Remote Sens., 4(12), 1573–1599, doi:10.3390/rs4061573, 2012.

Hastenrath, S. and Ames, A.: Diagnosing the imbalance of Yanamarey glacier in the Cordillera Blanca of Peru, J. Geophys. Res., 100(D3), 5105, doi:10.1029/94JD03108, 1995a.

Hastenrath, S. and Ames, A.: Recession of Yanamarey Glacier in Cordillera Blanca, Peru, during the 20th century, J. Glaciol., 41(137), 191–196, doi:10.1029/94JD03108, 1995b.

Hugenholtz, C. H., Whitehead, K., Brown, O. W., Barchyn, T. E., Moorman, B. J., LeClair, A., Riddell, K. and Hamilton, T.: Geomorphological mapping with a small unmanned aircraft system (sUAS): Feature detection and accuracy assessment of a photogrammetrically-derived digital terrain model, Geomorphology, 194, 16–24, doi:10.1016/j.geomorph.2013.03.023, 2013.

Huggel, C., Haeberli, W., Kääb, A., Hoelzle, M., Ayros, E. and Portocarrero, C.: Assessment of glacier hazards and glacier runoff for different climate scenarios based on remote sensing data : a case study for a hydropower plant in the Peruvian Andes, in EARSeL eProceedings, vol. 23, pp. 22–33., 2002.

Huh, K. I., Mark, B. G., Ahn, Y. and Hopkinson, C.: Volume change of tropical Peruvian glaciers from multi-temporal digital elevation models and volume–surface area scaling, Geogr. Ann. Ser. A, Phys. Geogr., 99(3), 222–239, doi:10.1080/04353676.2017.1313095, 2017.

Immerzeel, W. W., Kraaijenbrink, P. D. A., Shea, J. M., Shrestha, A. B., Pellicciotti, F., Bierkens, M. F. P. and De Jong, S. M.: High-resolution monitoring of Himalayan glacier dynamics using unmanned aerial vehicles, Remote Sens. Environ., 150, 93–103, doi:10.1016/j.rse.2014.04.025, 2014.

Juen, I., Kaser, G. and Georges, C.: Modelling observed and future runoff from a glacierized tropical catchment (Cordillera Blanca, Peru), Glob. Planet. Change, 59(1–4), 37–48, doi:10.1016/j.gloplacha.2006.11.038, 2007.

Juen, M., Mayer, C., Lambrecht, A., Han, H. and Liu, S.: Impact of varying debris cover thickness on ablation: A case study for Koxkar Glacier in the Tien Shan, Cryosphere, 8(2), 377–386, doi:10.5194/tc-8-377-2014, 2014.

Kaser, G.: Glacier-climate interactions at low latitudes, J. Glaciol., 47(157), 195–204, doi:10.3189/172756501781832296, 2001.

Kaser, G., Ames, A. and Zamora, M.: Glacier fluctuations and climate in the Cordillera Blanca, Peru, Ann. Glaciol., 14, 136–140, 1990.

Kaser, G., Juen, I., Georges, C., Gómez, J. and Tamayo, W.: The impact of glaciers on the runoff and the reconstruction of mass balance history from hydrological data in the tropical Cordillera Blanca, Peru, J. Hydrol., 282(1–4), 130–144, doi:10.1016/S0022-1694(03)00259-2, 2003.

Kaser, G., Großhauser, M., Marzeion, B. and Barry, R. G.: Contribution potential of glaciers to water availability in different climate regimes, Proc. Natl. Acad. Sci. U. S. A., 107(47), 21300–21305, doi:10.1073/pnas., 2010.

Koh, L. P. and Wich, S. A.: Dawn of drone ecology: low-cost autonomous aerial vehicles for conservation, Trop. Conserv. Sci., 5(2), 121–132, doi:WOS:000310846600002, 2012.

5   Kraaijenbrink, P., Meijer, S. W., Shea, J. M., Pellicciotti, F., De Jong, S. M. and Immerzeel, W. W.: Seasonal surface velocities of a Himalayan glacier derived by automated correlation of unmanned aerial vehicle imagery, Ann. Glaciol., 57(71), 103–113, doi:10.3189/2016AoG71A072, 2016.

Lejeune, Y., Bertrand, J.-M., Wagnon, P. and Morin, S.: A physically based model of the year-round surface energy and mass balance of debris-covered glaciers, J. Glaciol, 59(214), 327–344, doi:https://doi.org/10.3189/2013JoG12J149, 2013.

10   Lliboutry, L., Arnao, B. M., Pautre, A. and Schneider, B.: Glaciological problems set by the dangerous lakes in Cordillera Blanca, Peru. I. historical failures of morainic dams, their causes and prevention, J. Glaciol., 18(79), 239–254, 1977.

Lowe, D. G.: Distinctive image features from scale-invariant keypoints, Int. J. Comput. Vis., 60(2), 91–110, doi:10.1023/B:VISI.0000029664.99615.94, 2004.

Mark, B. G. and Seltzer, G. O.: Evaluation of recent glacier recession in the Cordillera Blanca, Peru (AD 1962-1999): Spatial
15   distribution of mass loss and climatic forcing, Quat. Sci. Rev., 24(20–21), 2265–2280, doi:10.1016/j.quascirev.2005.01.003, 2005.

Mark, B. G., Bury, J., McKenzie, J. M., French, A. and Baraer, M.: Climate change and tropical Andean glacier recession: Evaluating hydrologic changes and livelihood vulnerability in the Cordillera Blanca, Peru, Ann. Assoc. Am. Geogr., 100(4), 794–805, doi:10.1080/00045608.2010.497369, 2010.

Nex, F. and Remondino, F.: UAV for 3D mapping applications: A review, Appl. Geomatics, 6(1), 1–15, doi:10.1007/s12518-013-
20   0120-x, 2014.

Ostrem, G.: Ice melting under a thin layer of moraine, and the existence of ice cores in moraine ridges, Geogr. Ann., 41(4), 228–230 [online] Available from: http://www.jstor.org/stable/4626805, 1959.

Ostrem, G. and Brugman, M.: Glacier Mass-Balance Measurements: A Manual for Field and Office Work., 1993.

Portocarrero, C.: The Glacial Lake Handbook Reducing Risk From Dangerous Glacial Lakes in the Cordillera Blanca Peru, Peru,
25   United States Agency Int. Dev. Washington, DC, (February), 68, 2014.

Postigo, J. C., Young, K. R. and Crews, K. A.: Change and continuity in a pastoralist community in the high Peruvian Andes, Hum. Ecol., 36(4), 535–551, doi:10.1007/s10745-008-9186-1, 2008.

Pratap, B., Dobhal, D. P., Mehta, M. and Bhambri, R.: Influence of debris cover and altitude on glacier surface melting: A case study on Dokriani Glacier, central Himalaya, India, Ann. Glaciol., 56(70), 9–16, doi:10.3189/2015AoG70A971, 2015.

30   Rabatel, A., Francou, B., Soruco, A., Gomez, J., Caceres, B., Ceballos, J., Basantes, R., Vuille, M., Sicart, J.-E., Huggel, C., Scheel, M., Lejeune, Y., Arnaud, Y., Collet, M., Condom, T., Consoli, G., Favier, V., Jomelli, V., Galarraga, R., Ginot, P., Maisincho, L., Mendoza, J., Menegoz, M., Ramirez, E., Ribstein, P., Suarez15, W., Villacis, M. and Wagnon, P.: Current state of glaciers in the tropical Andes: a multi-century perspective on glacierevolution and climate change, Cryosph., 7(1), 81–102, doi:10.5194/tc-7-81-2013, 2013.

35   Racoviteanu, A. E., Arnaud, Y., Williams, M. W. and Ordoñez, J.: Decadal changes in glacier parameters in the Cordillera Blanca, Peru, derived from remote sensing, J. Glaciol., 54(186), 499–510, doi:10.3189/002214308785836922, 2008.

Reid, T. D. and Brock, B. W.: An energy-balance model for debris-covered glaciers including heat conduction through the debris layer, J. Glaciol., 56(199), 903–916, doi:10.3189/002214310794457218, 2010.

Reid, T. D., Carenzo, M., Pellicciotti, F. and Brock, B. W.: Including debris cover effects in a distributed model of glacier ablation,
40   J. Geophys. Res. Atmos., 117(17), doi:10.1029/2012JD017795, 2012.

Sakai, A., Nakawo, M. and Fujita, K.: Melt rate of ice cliffs on the Lirung Glacier, Nepal Himalayas, 1996, Bull. Glacier Res., 16(March 1998), 57–66, 1998.

Sakai, A., Takeuchi, N., Fujita, K. and Nakawo, M.: Role of supraglacial ponds in the ablation process of a debris-covered glacier in the Nepal Himalayas, in Debris-Covered Glaciers, edited by M. Nakawo, C. Raymond, and A. Fountain, pp. 119–130, Int. Asoc.
45   of Hydrological Sciences., 2000.

Schauwecker, S., Rohrer, M., Huggel, C., Kulkarni, A., Ramanathan, A. L., Salzmann, N., Stoffel, M. and Brock, B.: Remotely sensed debris thickness mapping of Bara Shigri Glacier, Indian Himalaya, J. Glaciol., 61(228), 675–688, doi:10.3189/2015JoG14J102, 2015.

Scherler, D., Bookhagen, B. and Strecker, M. R.: Spatially variable response of Himalayan glaciers to climate change affected by
50   debris cover, Nat. Geosci., 4(3), 156–159, doi:10.1038/ngeo1068, 2011.

Shahi, S., Kayastha, R. B., Baral, P. and Mool, P. K.: Influence of a debris layer on the melting of ice on Lirung glacier, Langtang valley, Rasuwa, Nepal, J. Hydrol. Meteorol., 9(1), 95–108, 2015.

Shroder, J. F., Bishop, M. P., Copland, L. and Sloan, V. F.: Debris-covered Glaciers and Rock Glaciers in the Nanga Parbat Himalaya, Pakistan, Geogr. Ann. Ser. A, Phys. Geogr., 82(1), 17–31, doi:10.1111/j.0435-3676.2000.00108.x, 2000.

Snavely, N., Seitz, S. M. and Szeliski, R.: Modeling the world from Internet photo collections, Int. J. Comput. Vis., 80(2), 189–210, doi:10.1007/s11263-007-0107-3, 2008.

5   Szeliski, R.: Computer Vision : Algorithms and Applications, Computer (Long. Beach. Calif)., 5, 832, doi:10.1007/978-1-84882-935-0, 2010.

Thompson, S. S., Benn, D. I., Dennis, K. and Luckman, A.: A rapidly growing moraine-dammed glacial lake on Ngozumpa Glacier, Nepal, Geomorphology, 145–146, 1–11, doi:10.1016/j.geomorph.2011.08.015, 2012.

Verhoeven, G.: Taking computer vision aloft - archaeological three-dimensional reconstructions from aerial photographs with
10   photoscan, Archaeol. Prospect., 18(1), 67–73, doi:10.1002/arp.399, 2011.

Vivoni, E. R., Rango, A., Anderson, C. A., Pierini, N. A., Schreiner-McGraw, A. P., Saripalli, S. and Laliberte, A. S.: Ecohydrology with unmanned aerial vehicles, Ecosphere, 5(10), art130, doi:10.1890/ES14-00217.1, 2014.

Vuille, M., Bradley, R. S., Werner, M. and Keimig, F.: 20th century climate change in the tropical Andes: Observations and model results, Clim. Change, 59(1–2), 75–99, doi:10.1023/A:1024406427519, 2003.

15   Vuille, M., Kaser, G. and Juen, I.: Glacier mass balance variability in the Cordillera Blanca, Peru and its relationship with climate and the large-scale circulation, Glob. Planet. Change, 62(1–2), 14–28, doi:10.1016/j.gloplacha.2007.11.003, 2008.

Watts, A. C., Ambrosia, V. G. and Hinkley, E. A.: Unmanned aircraft systems in remote sensing and scientific research: Classification and considerations of use, Remote Sens., 4(6), 1671–1692, doi:10.3390/rs4061671, 2012.

Whitehead, K., Moorman, B. J. and Hugenholtz, C. H.: Brief Communication: Low-cost, on-demand aerial photogrammetry for
20   glaciological measurement, Cryosphere, 7(6), 1879–1884, doi:10.5194/tc-7-1879-2013, 2013.

Winkler, M., Juen, I., Mölg, T., Wagnon, P., Gómez, J. and Kaser, G.: Measured and modelled sublimation on the tropical Glaciar Artesonraju, Per, Cryosph., 3(1), 21–30, doi:10.5194/tc-3-21-2009, 2009.

Young, K. R.: Andean land use and biodiversity: humanized landscapes in a time of change, Ann. Missouri Bot. Gard., 96(3), 492–507, doi:10.3417/2008035, 2009.

25   Young, K. R.: Ecology of land cover change in glaciated tropical mountains, Rev. Peru. Biol., 21(3), 259–270, doi:10.15381/rpb.v21i3.10900, 2014.

Tables

Survey Year	Ground Target Used	Number of Targets	Number of Check Points	Base Station	Rover
2014	10 inch diameter plastic plates; sprayed florescent yellow, silver taped X for centre	14	18	Trimble 5700 L1/L2 Receiver; Trimble Zephyr Geodetic Antenna (UNAVCO)	Topcon GRS1 L1 Receiver, Topcon PG-A1 External Antenna
2015	12 inch square floor tiles; side a: yellow coroplast pink X centre; side b: black and white quads	11	13	Topcon Hiper SR L1/L2 Integrated Receiver and Antenna	Topcon GRS1 L1 Receiver, Topcon PG-A1 External Antenna

Table 1: Llaca glacier GNSS ground control survey and hardware specifications.

GNSS Survey Error Estimates	July 23, 2014	July 28, 2015
Base Station Observation Length	>106 Hours	6.5 Hours
Rover Observation Length	5 mins	5 mins
Base Station and Rover Observation Rate	1 Hz	1 Hz
Average Horizontal Baseline Length	14.9 km	1.2 km
Average Vertical Baseline Length	1400 m	9 m
Base Station Horizontal Confidence (95%)	0.0022 m	0.0326 m
Base Station Vertical Confidence (95%)	0.004 m	0.041 m
Total GCP Horiz. Er. Estimate (Rover RMS + Base Station)	0.017 m	0.035 m
Total GCP Vert. Er. Estimate (Rover RMS + Base Station)	0.019 m	0.045 m
Total Check Pt Horiz. Er. Estimate (Rover RMS + Base Station)	0.011 m	0.035 m
Total Check Pt Vert. Er. Estimate (Rover RMS + Base Station)	0.020 m	0.044 m

Table 2: Estimated GNSS survey positional errors for use in SfM ground control and absolute DEM error analysis. Note: Total error estimates include base station and rover error estimates.

	July 23, 2014	July 28, 2015
Number of Images Captured	601	929
Number of Images Used	323	826
Av. Flying Altitude	110.46 m	116.11 m
Ground Resolution	0.0353 m/pixel	0.0367 m/pixel
Coverage Area	0.489 km^2	0.542 km^2

30

Table 3: UAV Photogrammetric survey parameters.

35

	July 23, 2014	July 28, 2015
Tie Points	84530	53545
Projections	387568	357433
Tie Point Matching Error	0.632 pixels	0.430 pixels
GCP X Error	0.0009 m	0.0019 m
GCP Y Error	0.0007 m	0.0017 m
GCP Z Error	0.0012 m	0.0005 m
GCP Total Error	0.0016 m	0.0026 m
GCP Total Error	0.0809 pixels	0.0231 pixels
Max DEM Resolution	0.071 m/pixel	0.073 m/pixel
Point Cloud Density	200 points/m^2	185 points/m^2

Table 4: Estimated pixel matching and DEM reconstruction errors from SfM processing workflow.

Figures
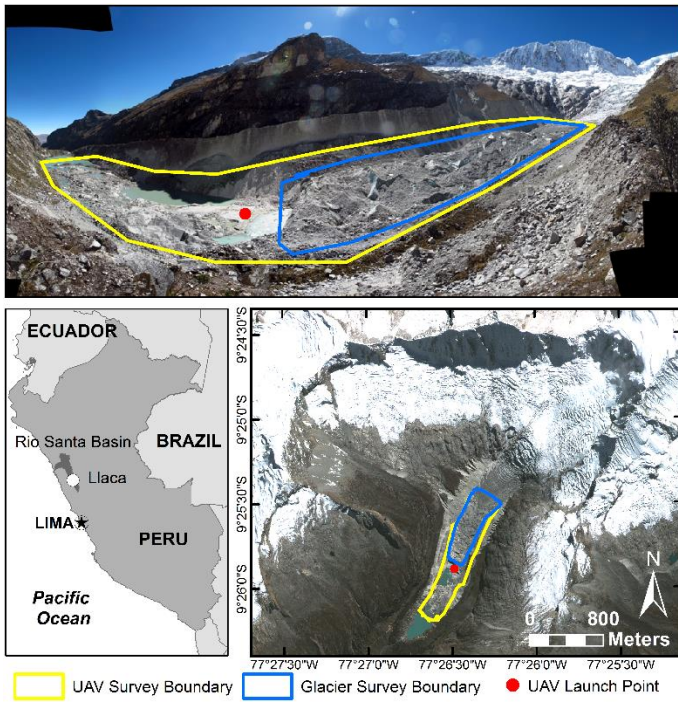
Figure 1: Llaca glacier location map within the Cordillera Blanca. Showing UAV launch point and survey area boundaries. UAV survey boundary (yellow line) is maximum extent of study area covered by both 2014 and 2015 surveys; Glacier survey boundary (blue line) is maximum extent of glacier tongue covered by both 2014 and 2015 surveys.

Figure 2: GNSS survey at Llaca glacier (left), installed ground control target (2015) (top right), hexacopter UAV platform used in this study (bottom right).
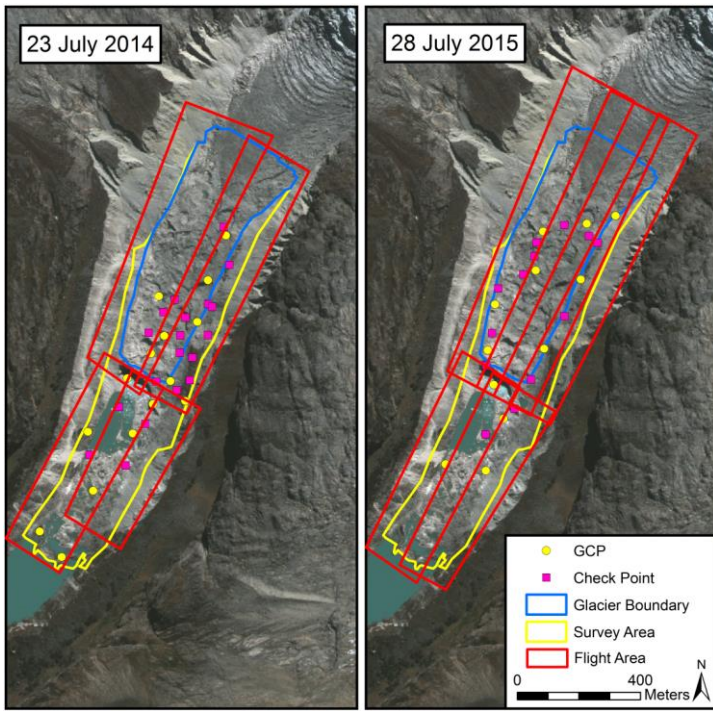
Figure 3: Flight coverage areas, GCP's and check point locations for 2014 and 2015 UAV survey campaigns. Background imagery from Worldview 13 July, 2011.
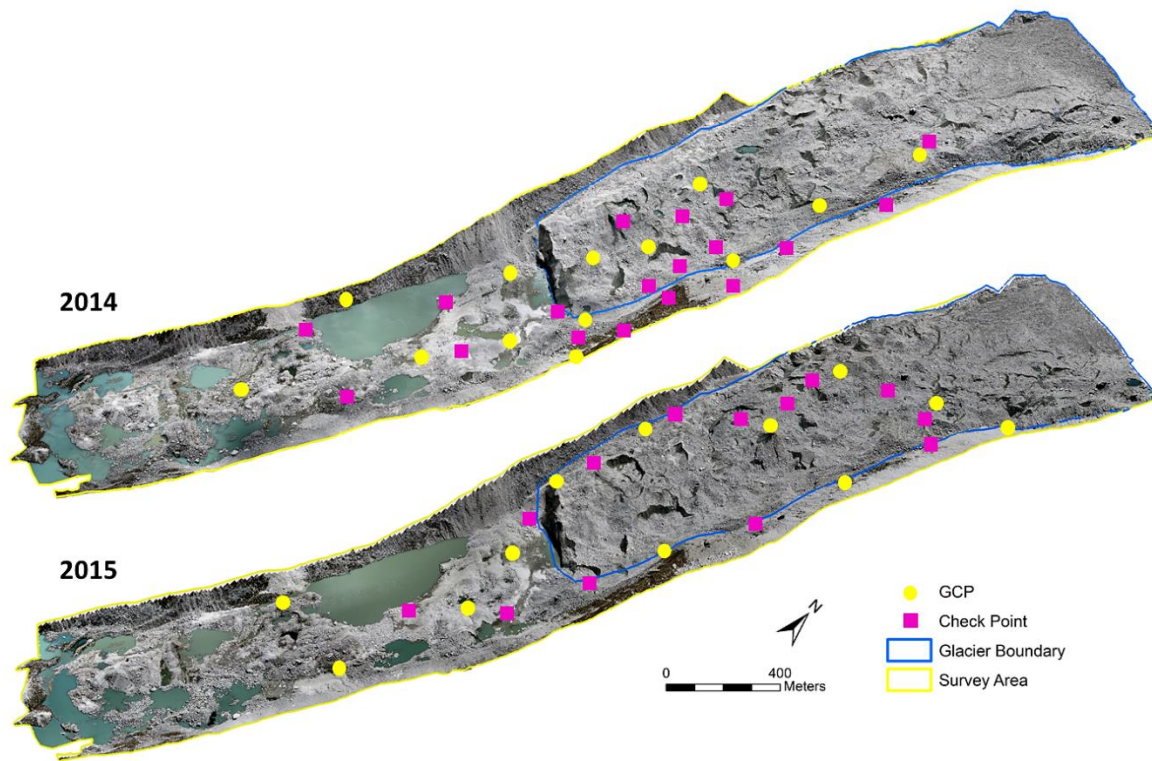
Figure 4: Photogrammetric DEM's and RGB orthomosaics of Llaca glacier tongue in 2014 (top) and 2015 (bottom), constructed through SfM workflow.
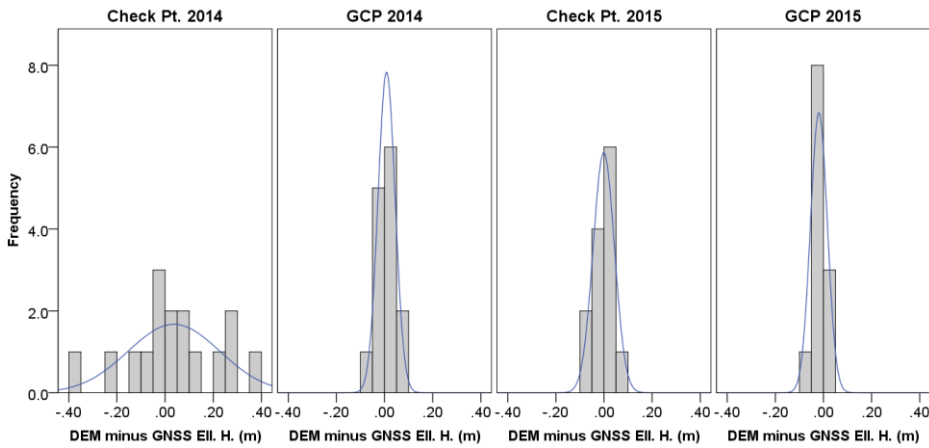
Figure 5: Histogram plot of elevation differences (errors) between check points and GCP surveyed elevations and DEM elevations for 2014 and 2015 respectively Note: negative values indicate underestimation of DEM surface with respect to surveyed positions and thus imply flattening of the DEM surface. Most errors are less than +/-5cm and all within +/-10cm except for 2014 check points. Large 2014 check point errors are assumed to be the result of poor location selection.
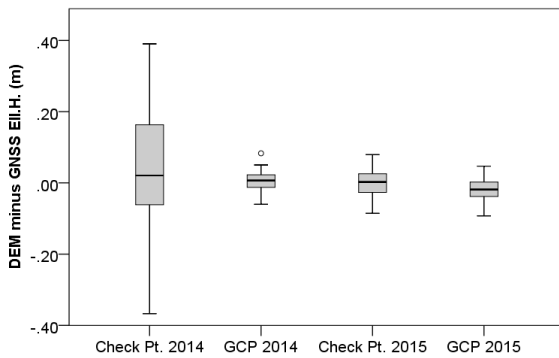
Figure 6: Box and whisker plot of elevation differences (errors) between check points and GCP surveyed elevations and DEM elevations for 2014 and 2015 respectively. Thick lines represent median value, boxes show upper and lower quartiles and whiskers indicate minimum and maximum values, circles are outliers. Note: negative values indicate underestimation of DEM surface with respect to surveyed positions and thus imply flattening of the DEM surface. Most errors are less than +/-5cm and all within +/-10cm except for 2014 check points. Large 2014 check point errors are assumed to be the result of poor location selection.
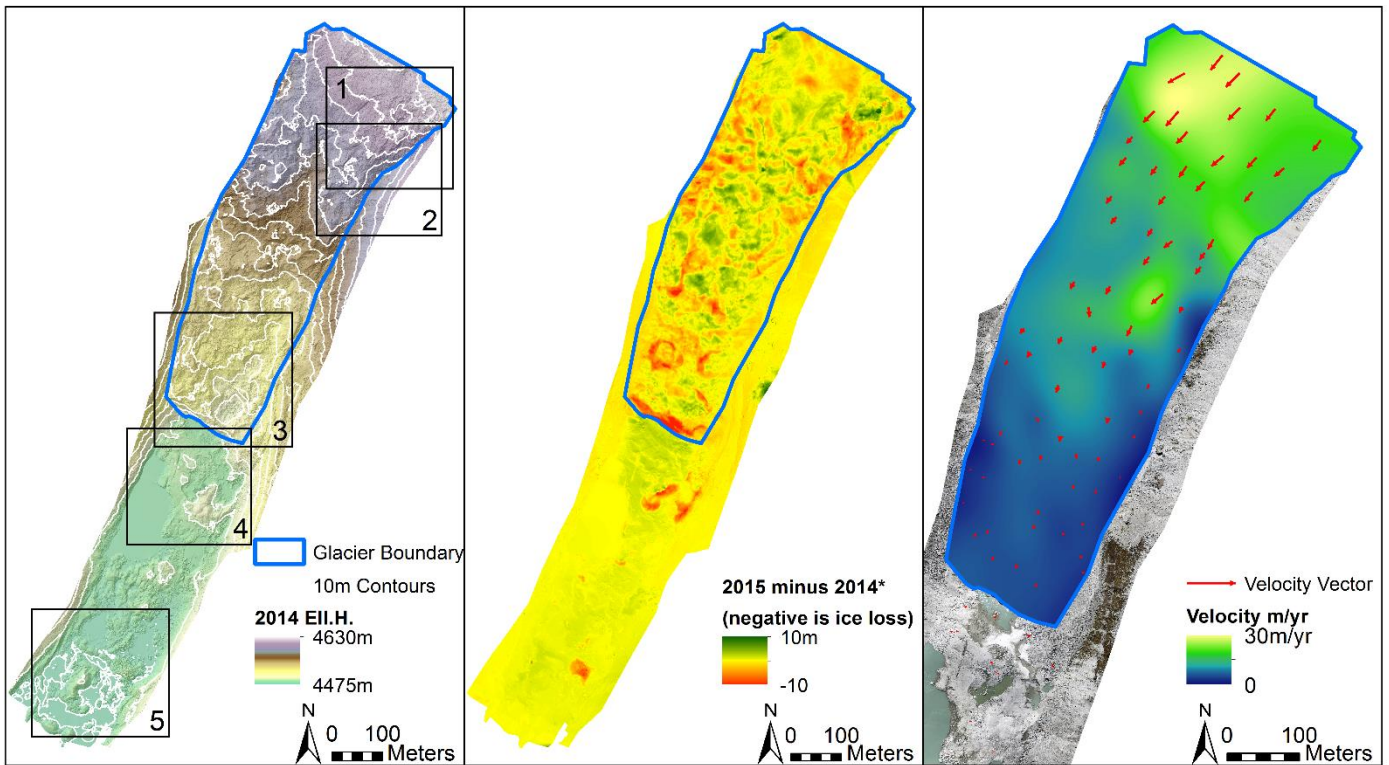
Figure 7: 2014 SfM DEM elevations (Ell.H.) (left); Vertical change in elevation from 23 July 2014 to 28 July 2015 (centre); Glacier surface velocity tracks and interpolated velocity surface (right). Numbered extent boxes depict locations of: 1 – Figure 9 right panels; 2 - Figure 11 top panels; 3 - Figure 9 left panels and Figure 11 lower panels; 4 - Figure 13 left panels; 5 - Figure 13 right panels. *Note: centre panel values are truncated to +/-10m for display purposes (see Figure 8).
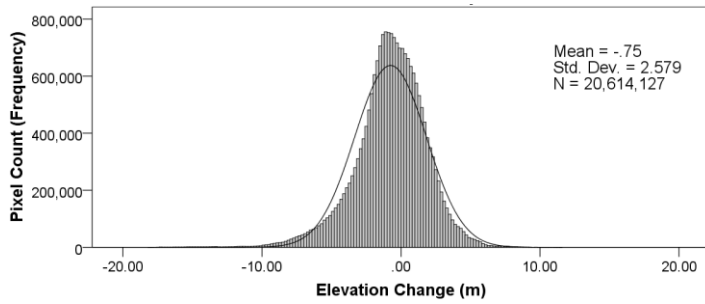
Figure 8: Histogram of measured elevation changes over glacier tongue (blue boundary in Figure 7) from 23 July 2014 to 28 July 2015. Calculated from subtraction of 2014 DEM from 2015 DEM (i.e. negative values are ice loss) at 10cm DEM pixel size.
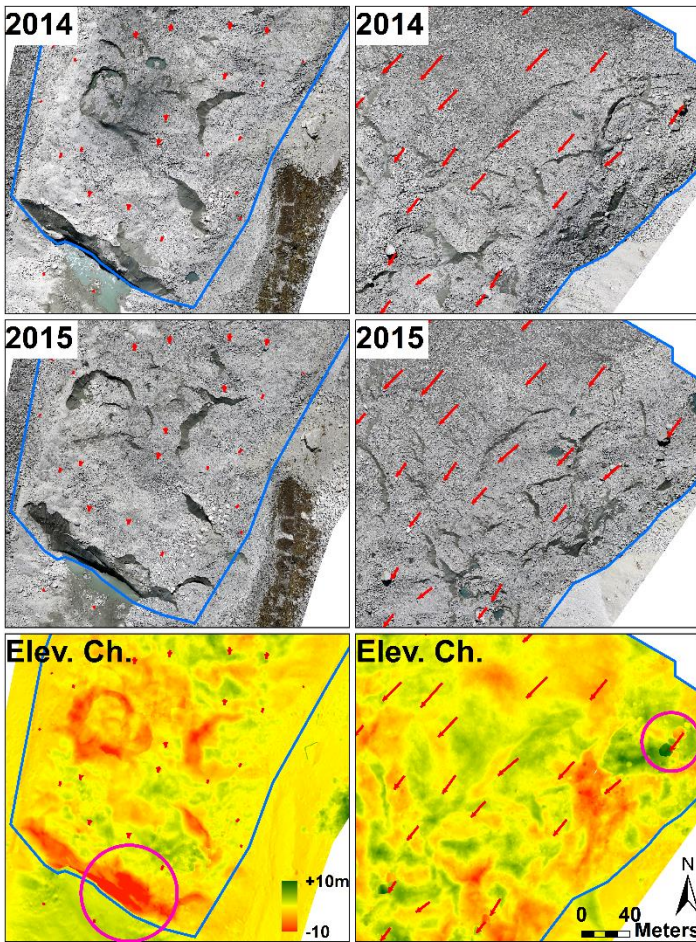
Figure 9: Locations of maximum and minimum change in ice elevation on Llaca glacier tongue. Upper row panels show 2014 orthomosaic; middle row panels show 2015 orthomosaic; lower row panels show elevation change where 2014 elevation is subtracted from 2015 elevation (i.e. negative value is ice loss). Maximum ice loss of 18m occurred at the calving face (pink circle lower left panel). Maximum gain of 11m is recorded in upper right section where a large boulder (roughly 10m tall) has moved through the scene (visible by comparison of 2014 and 2015 orthomosaics). Blue line is glacier tongue boundary, red arrows are velocity measurements. Note: elevation change values are truncated to +/-10m for display purposes. Location of panels is depicted in Figure 7 inset boxes: 3 – left panels; 1 – right panels.
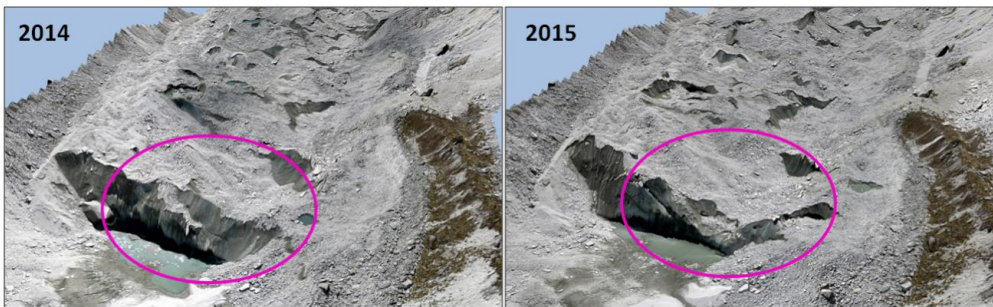
Figure 10: Collapse of the calving face.
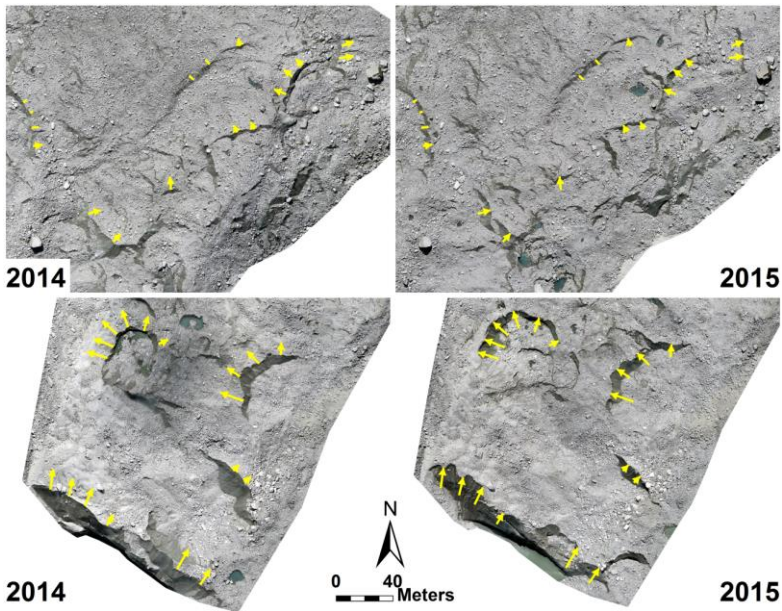
Figure 11: Rapid ice loss around exposed ice cliffs and surface melt ponds.Top row images are from upper right of surveyed area, lower row images are behind calving face. Yellow arrows indicate horizontal movement of feature from 2014 to 2015 of ice cliff position; 2-25m/year. More rapid retreat of ice cliffs is observed in the lower glacier, where cliffs are larger and temperatures are warmer. NOTE: 2015 images have been shifted (georectified) to 2014 positions based on velocity vectors (Figure 7), i.e. horizontal glacier movement is removed so that the same location relative to glacier surface is compared. Location of panels is depicted in Figure 7 inset boxes: 2 – upper panels; 3 – lower panels.
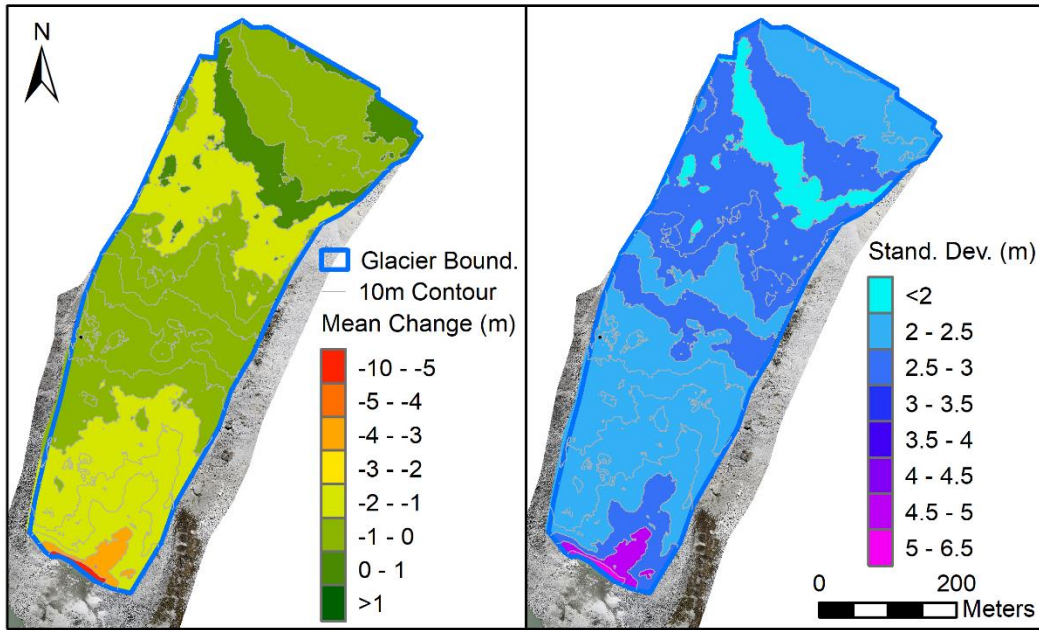
Figure 12: Changes in glacier tongue elevation by 10m elevation band. Left: mean elevation change within a 10m elevation band. Right: standard deviation of elevation change within a 10m elevation band.
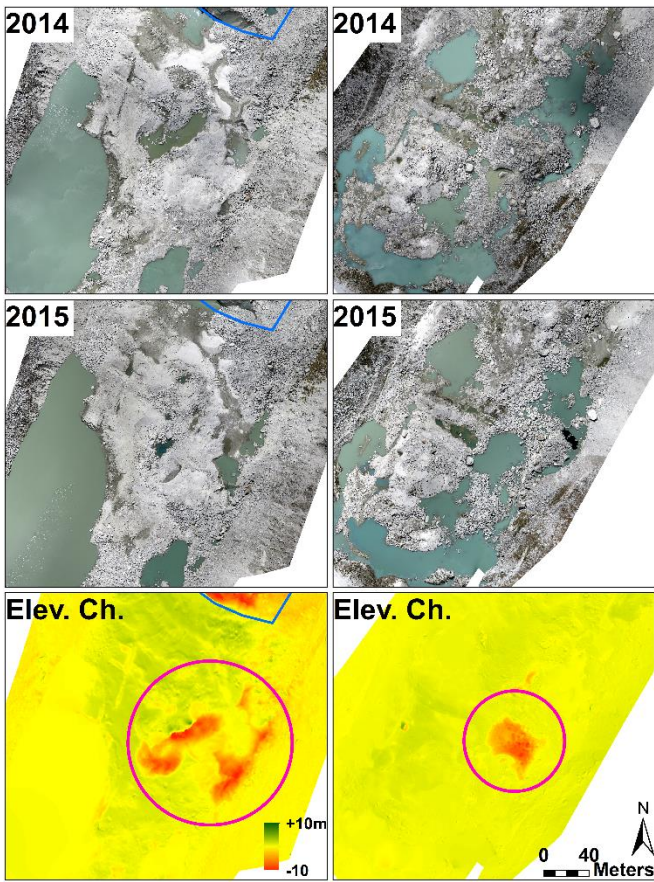
Figure 13: Locations of major elevation change (ice loss) within lake sediments (pink circles), indicate buried glacier ice is still present. Low surface velocities were also measured here (~2.5m/yr below calving face in left panels, and ~0.5m/yr at end of surveyed region in right panels, indicating these sediments are still connected to the main glacier tongue. Upper row panels show 2014 orthomosaic; middle row panels show 2015 orthomosaic; lower row panels show elevation change where 2014 elevation is subtracted from 2015 elevation (i.e. negative value is ice loss). Blue line is glacier tongue boundary. Note: elevation change values are truncated to +/-10m for display purposes. Location of panels is depicted in Figure 7 inset boxes: 4 – left panels; 5 – right panels.